LBL-11857 1/2
Preprint

Lawrence Berkeley Laboratory
UNIVERSITY OF CALIFORNIA

Materials & Molecular Research Division

Submitted to the Journal of the American Ceramic Society

SINTERING OF MULLITE-CONTAINING MATERIALS:
I. EFFECT OF COMPOSITION

Michael D. Sacks and Joseph A. Pask

December 1981

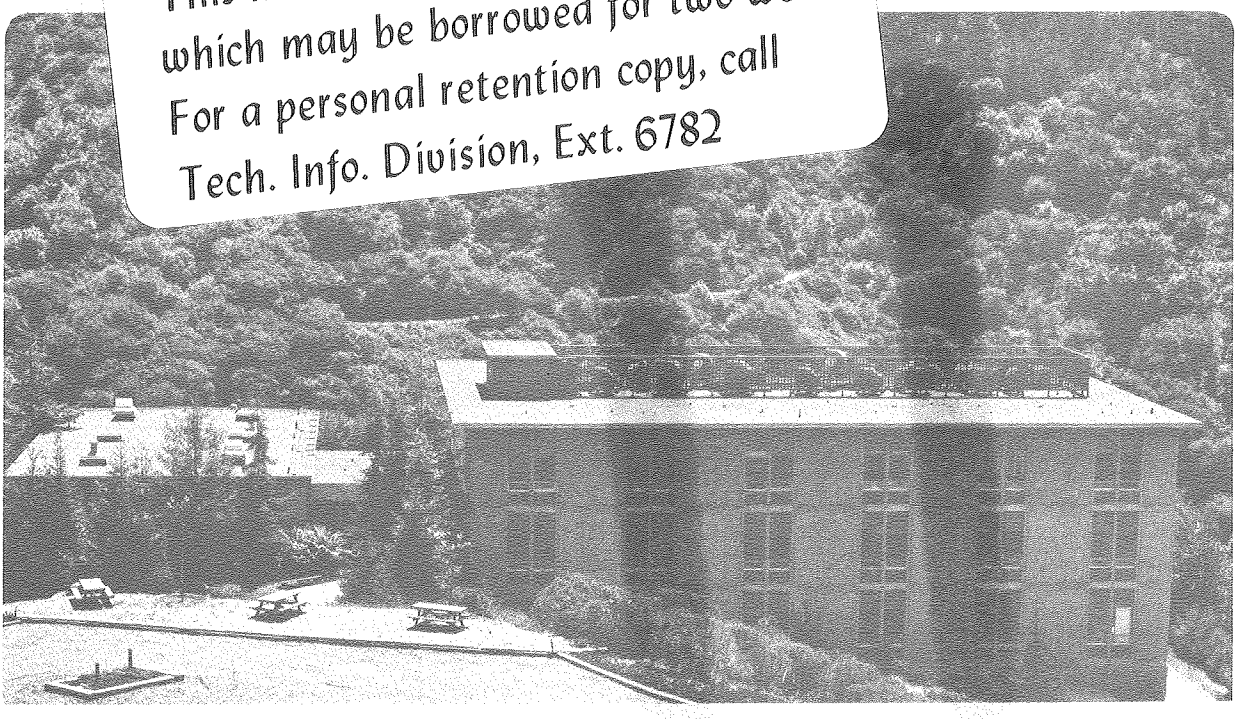

Prepared for the U.S. Department of Energy under Contract DE-AC03-76SF00098

DISCLAIMER

SINTERING OF MULLITE-CONTAINING MATERIALS:

I. EFFECT OF COMPOSITION

Michael D. Sacks* and Joseph A. Pask

Department of Materials Science and Mineral Engineering and
Materials and Molecular Research Division of
Lawrence Berkeley Laboratory, University of California
Berkeley, CA 94720

ABSTRACT

Sintering behavior of mullite-containing powders was studied over a range of chemical compositions (Al_2O_3/SiO_2 ratio). Densification measurements were made for both liquid phase-containing and solid state systems. Small amounts of liquid phase were observed to have a significant effect on densification rate. A linear relationship was obtained between the percent of theoretical density and the logarithm of time for compositions in the range 73-75 wt% Al_2O_3. Currently available models for intermediate stage sintering kinetics were considered to be inadequate for these systems. Grain boundary transport or diffusion appeared to be the primary mechanism of densification.

This work was supported by the Director, Office of Energy Research, Office of Basic Energy Sciences, Materials Science Division of the U.S. Department of Energy under Contract No. DE-AC03-76SF00098.

*Now with Department of Materials Science and Engineering, University of Florida, Gainesville, Florida 32611.

I. INTRODUCTION

Sintering is usually divided into three stages - initial, intermediate, and final - based on the geometrical changes that occur in the densifying powder compact. The intermediate stage of sintering is of great importance in the controlled development of ceramic microstructures since most of the densification occurs during this stage. This regime is characterized in real systems by the (1) occurrence of grain growth and (2) nonuniform evolution of the porosity from continuous open channels along grain boundaries to discrete, isolated closed pores at grain corners. Although many factors, including the mass transport mechanisms, powder compact characteristics, sintering environment, etc., are known to influence sintering kinetics, their combined effect on the specific time dependence of densification observed during the intermediate stage is not well understood.

In this study, densification kinetics, with emphasis on the intermediate stage, were obtained for several aluminum silicate compositions containing mullite as the primary phase. Recent studies[1-5] have shown that only a fraction of mullite's potential capabilities in regards to mechanical strength, creep resistance, and acid corrosion resistance, are achieved in normal processing due primarily to the presence of a liquid or glassy film along grain boundaries. In order to improve properties and to understand sintering behavior, studies which relate processing variables to microstructural evolution (including kinetics) are of importance.

II. Experimental Procedure

1) Starting Materials and Processing

Starting materials were A-14 aluminum oxide (α-Al_2O_3) and silica flour (α-quartz) which had purities of ∿99.8% and ∿99.6%, respectively. Semiquantitative spectrographic analyses[Δ] showed that the major impurity in the A-14* was SiO_2 and the major impurity in the silica flour[†] was Al_2O_3.[(6)]

Compositions ranged from 60 wt% Al_2O_3/40 wt% SiO_2 to 90 wt% Al_2O_3/10 wt% SiO_2. Mixing and de-agglomeration were achieved by wet (isopropyl alcohol) milling in (1) a porcelain ball mill (mixing condition "I") or (2) a teflon-lined vibratory mill[Π] (mixing condition "P"). After stir-drying and screening (-120 mesh), mixtures were calcined at 1700°C for 8 hrs to form mullite, mullite and aluminum silicate glass, or mullite and alumina (depending on the overall Al_2O_3/SiO_2 ratio - see the stable phase equilibrium diagram, Fig. 1).

After calcination, mixtures were subjected to coarse crushing in a mechanically operated mortar and pestle, and wet (isopropyl alcohol) vibratory milling (grinding condition "P") for 5 hours. After stir-drying

---

Δ American Spectrographic Laboratories, Inc., S.F., Ca.

* Alcoa Aluminum Co., Bauxite, Ark. Spectrographic analysis: Si .035%, Na <.02%, Ca .02%, Mg .001%, Ti .005%, Fe .03%, Ga .01%, Zr .01%, Cu <.001%, Mn <.001%, Cr <.001%, B .01%.

† Ottawa Silica Co., Ottawa, Ill. Spectrographic analysis: Al .2%, Na <.02%, Ca .02% Mg .035%, Ti .025%, Fe .05%, Zr .003%, Cu <.001%, Ba .004%, Mn <.001%, Cr .001%, B .01%, Pb <.005%, Sr .005%, Ni <.001%

Π Sweco, Inc., Los Angeles, Ca.

∇ Pulverisette, Alfred Fritsch Co., W. Germany

and screening (-120 mesh), powders were calcined at 800°C for 1 hr to volatilize any organic contamination. Powders were labeled according to composition and mixing/grinding conditions, e.g. 73IP refers to 73 wt% Al_2O_3 composition mixed by condition "I" and ground by condition "P". Semi-quantitative spectrographic analyses showed[6] that processing introduces no additional cationic impurities and that, within experimental precision, the total cationic impurity is the same in all compositions (~.2-.3 wt%). X-ray diffraction and microscopy have shown, however, that α-Al_2O_3 is introduced by impact collisions during vibratory milling (high density alumina grinding media** were used); therefore, the "PP" compositions have the largest Al_2O_3 contamination as particles of α-Al_2O_3.

Powder compacts were formed under uniaxial pressure ($\sim 17 MN/m^2$) followed by isostatic pressing at $\sim 170 MN/m^2$.

2) Sintering Conditions

Compacts were sintered under isothermal conditions in an electrically heated quench-type furnace with $MoSi_2$ elements†† in static air. The temperature was monitored and controlled by a Speedomax - H Recorder Series 60 Controller$^{\Delta\Delta}$ with Pt 6%Rh - Pt 30%Rh thermocouples.

3) Properties

"Average" particle size and surface area of powders were determined by an air permeability method$^{\text{III}}$ and by a multipoint BET adsorption method***, respectively.

** Norton Co., Akron, Ohio
Coors Procelain Co., Golden, Col.

†† Kanthal Corp., Bethel, Conn.

$\Delta\Delta$ Leeds and Northrup Co., Philadelphia, PA.

III Fisher Subsieve Sizer, Fisher Scientific Co., Pittsburg, PA.

*** Quantasorb, Quantachrome Corp., Greenvale, N.Y.

Bulk density and open porosity were determined by the displacement method utilizing distilled water. Percent of theoretical density (% ρ_{th}) was determined by using the apparent true density obtained from green compacts. In green compacts, the total porosity $\approx$ open porosity; the latter quantity is measurable by the displacement method.

High temperature (1200° and 1400°C) stress-strain testing under compression was carried out on several samples. Experimental details have been described elsewhere.(3)

4) Microscopy

Standard ceramographic procedures were followed to obtain sections for microstructural observations on sintered compacts. Samples were observed by scanning electron microscopy (SEM)****, transmission electron microscopy (TEM)ΠΠΠΠ, and in reflected light by interference-contrast microscopy†††. A light etch with diluted hydrofluoric acid solution and/or a thin gold coating were helpful in bringing out features viewed in the optical microscope. Polished samples for viewing by SEM were thermally etched (1400-1550°C, depending on initial sintering conditions) in order to make grain boundaries visible. Etching was followed by coating with a thin gold layer. An EDAX∇∇ (Energy Dispersive Analysis by X-rays) attachment was used to detect free α-Al_2O_3 particles.

**** AMR 1000, Advanced Metals Research Co., Bedford, Mass.

ΠΠΠΠ Philips 301, Philips Co., Amsterdam.

††† Nomarsky Differential Interference - Contrast Microscopy, Zeiss Ultraphot II, Metallograph, Carl Zeiss Co., W. Germany.

∇∇ North American Philips Corp., Curryview, Ill.

III. Results

1) Effect of Composition on Densification

In order to get a basic understanding of the system, a broad composition range, 60 to 90 wt% Al_2O_3, was used in the initial experiments.[7] The green density and "average" particle size were held approximately constant over the composition range (57 ± 1 $\%\rho_{th}$ and 2.1 ± 0.2 μm, respectively). Figure 2 shows plots of the percent of theoretical density versus composition for samples sintered at 1700°C for 1, 4, and 12 hrs. Three groupings can be delineated:

1) 60IP and 65IP, in the mullite and liquid phase region at 1700°C of the equilibrium Al_2O_3-SiO_2 phase diagram (Fig. 1), sinter in 1 and 4 hr, respectively, to maximum density due to the presence of large amounts of liquid (Fig. 3) at the sintering temperature.
2) 71.8IP, 73IP, and 74IP (in the mullite solid solution range - see Fig. 1) sinter at a slower rate but achieve a high density (12 hr fire).
3) Compositions with 75 wt% Al_2O_3 and above sinter even more slowly. A sharp decrease in densification rate is observed between 74IP and 75IP. The boundary between the mullite solid solution and the mullite and alumina phase regions (M-MA phase boundary) is at ∿74 wt% Al_2O_3 at 1700°C.

2) Densification Kinetics

More detailed densification kinetics were studied on the compositions listed in Table 1.[7] The surface area and "average" particle size of the powder, and green density were kept approximately constant. The 60IP

composition showed only mullite in the x-ray diffraction pattern since the aluminum silicate glass phase is not detected. 73PP was subjected to the largest composition shift during processing (due to Al_2O_3 contamination during both vibratory milling and mixing) so that a trace of α-Al_2O_3 was detected by x-ray diffraction after calcination. 75IP had a small amount of α-Al_2O_3 which was expected since the composition lies in the mullite and alumina phase region.

Figure 4 shows plots of percent of theoretical density vs. time at 1660°C for the four compositions. Densification is very rapid for 60IP due to presence of a large amount of liquid phase. Densification rate decreases with increasing alumina content. The decrease from 73IP to 73PP indicates that the overall alumina content for the latter sample has shifted during processing (from milling with Al_2O_3 media) to a composition close to the M-MA phase boundary.

Figures 5, 6, and 7 show plots of percent of theoretical density vs. logarithm of time for compositions 73IP, 73PP, and 75IP, respectively. A proportionality between $\%\rho_{th}$ and ℓn time is observed over a range of densities from $\sim 60\%\rho_{th}$ to $\sim 90 - 95\%\rho_{th}$ in each case (60IP did not follow this relationship). The decreasing slopes at high densities (above $\sim 90 - 95\%\rho_{th}$) correspond to the transition from intermediate to final stage sintering. Figure 8 (73IP sample) shows that the porosity present above $\sim 95\%\rho_{th}$ consists entirely of closed pores; it also indicates that the pore structure is related to density irrespective of temperature of firing.

IV. Discussion

1) Change in Densification Rate at the M-MA Boundary

In a compound with a solid solution range, the densification kinetics may be modified if changes in defect concentration of the slower diffusing species occur when the composition is altered. This possibility does not appear to be an important factor in the present study since no significant changes in densification behavior occur across the solid solution range of mullite, as indicated by the second grouping in Fig. 2.

Microstructural observations suggest that the sizable decrease in densification kinetics upon entering and traversing the M-MA phase boundary region is associated with the elimination of a residual glassy (nonequilibrium) phase. A feature of interest in the 73IP and 74IP samples (Fig. 9) are the rectangular - shaped grains, forming unusual dihedral angles, which suggest the presence of a liquid "film" along some grain boundaries at the sintering temperature. Further evidence of glass "films" is shown in the TEM micrograph of a 73IP sample in Fig. 10 (bottom). Small, angular second phase "pockets" are also observed in Fig. 10 (top). Noncrystallinity of these areas was indicated by the observation of diffuse rings in the electron diffraction patterns of these areas.

Further evidence that these second phase areas are amorphous is given by the stress-strain behavior in compression loading at 1200°C (Table 2). 71.8IP, 73IP, and 74IP are similar in important microstructural features (grain size and density), yet the strength increases with higher Al_2O_3 composition. The increase in strength can be accounted for by a

decreasing glass phase content. The 75IP sample also supports these conclusions because, despite a lower density ($83\%\rho_{th}$ vs. $95\%\rho_{th}$), the apparently glass-free 75IP specimen is still as strong as the glass-containing 71.8IP sample. The expected more severe deleterious effect of small amounts of glass phase on strength at higher temperatures is confirmed in strength tests performed at 1400°C (Table 2); in comparison with 1200°C values, the decrease in strength for 71.8IP is 60% and for 74IP (with a lesser amount of liquid), 25%. Therefore, despite relatively pure materials and long reaction times, it appears that a glass phase, though decreasing to very small amounts, exists in the compositions within the mullite solid solution range until free α-Al_2O_3 begins to appear. The reason for this behavior is uncertain. However, it provides an explanation for the decreased sintering rate on transition from 74IP to 75IP.

The possibility that glass phase exists due to insufficient calcination time (i.e. resulting in incomplete reaction) has been considered. Free Al_2O_3 introduced by grinding after calcination can be used as an indication of the completeness of reaction. Occasional α-Al_2O_3 particles are present in 73IP samples after sintering at low temperatures for short times (1580°C for 1 hr) as seen in Fig. 11. However, particles are not in evidence at higher temperatures and longer times of sintering, yet the micrographs indicating a glass phase (Figs. 9 and 10) were for samples sintered at 1700°C for 12 hrs. Further evidence against the argument of incomplete reaction is indicated in Figs. 12 and 13. The top micrograph in Fig. 12 shows the presence of glass phase in a 71.8IP sample which had been sintered at 1700°C for 8 hr. The sample in the bottom micrograph, also fired at 1700°C for 8 hr, had an overall composition of 75 wt% Al_2O_3

(just to the right of the M - MA phase boundary). The sample used in this case was formed by adding enough A-14 alumina to the 71.8IP powder to bring the composition up to 75 wt% Al_2O_3. Despite the relatively large size of the alumina particles (~3 μm), the glass phase appears to be effectively eliminated during firing. This assumption is supported by the curvature of the grain boundaries and the nature of the dihedral angles (Fig. 12B). Furthermore, on sintering the 71.8 IP sample for 100 hrs at 1700°C, the glass phase coalesced into large (up to ~10 μm in a linear dimension) "pockets" (Fig. 13) instead of being absorbed by the mullite grains (Fig. 1). Therefore, it does not appear that the presence of liquid phase is due to straightforward incomplete reaction. Also, the absence of liquid phase at 75 wt% indicates that its appearance in lower alumina-content specimens (71.8, 73 and 74) is not due to impurities in the raw materials.

An explanation which would account for the observed results is the existence of a metastable assemblage of high Al_2O_3 mullite (74.5 wt% Al_2O_3, i.e. the composition at the M - MA boundary) and the observed glass phase. Based upon structural considerations[8-9] and observations of elongated morphologies,[3,10-12] a high degree of surface energy anisotropy may be expected for mullite. The persistence of a silicate glass along high energy grain boundaries would be favorable since its presence would be expected to lower the interfacial energies; it could be further postulated that this condition could stabilize the configuration. Since α-Al_2O_3 is not observed in samples with a glassy phase, the Al_2O_3 content in the mullite would have to be higher in order to obtain the overall chemical composition. Chemical analysis of the individual mullite grains

would be required to rigorously test this hypothesis. The existence of metastable mullite crystals with high alumina contents (up to ~83 wt%) has been well documented[11,13], but this documentation applies to crystals that have precipitated from aluminum silicate melts on cooling.

2) Significance of the $\%\rho_{th}$ - ℓn Time Proportionality

The observation of a proportionality between $\%\rho_{th}$ and ℓn time for 73IP, 73PP, and 75IP (Figs. 5-7) is consistent with the results of several other systems[14-17] during intermediate stage sintering. However, other time dependencies of densification have also been reported for intermediate stage sintering.[17-21]

The predicted time dependence of densification for intermediate stage sintering of the different models[21-27] varies with the proposed mass transport mechanisms or combinations of mechanisms. Several models[23-26] indicate a semi-logarithmic relationship between $\%\rho_{th}$ and time under certain conditions pertaining to the geometry and the mechanisms operative during sintering. Although the assumptions made in deriving these models are tremendously different, each predicts the ℓn time dependence of densification only when volume diffusion is the mass transport mechanism. However, in the present study, grain boundary transport appears to be the primary mass transport mechanism responsible for densification. This argument is supported by the fact that the same time dependence of densification is observed for 73IP samples, with small amounts of glass phase and grain boundary "films", and for 75IP samples (with no glass phase). The higher densification rate for 73IP (relative to 75IP) is attributed to enhanced transport along glass-containing grain boundaries in 73IP (i.e. due to an

increased effective grain boundary diffusion coefficient), as opposed to a particle rearrangement stage[28]. Particle rearrangement is not considered important in 73IP because the amount of glassy phase is small. The semi-logarithmic relationship between $\%\rho_{th}$ and time is not observed when a significant amount of liquid phase is present, such as in 60IP.[6] Extremely rapid densification is observed[6] which can be attributed to solid particles sliding over one another and to the collapse of particle bridges under the action of capillary pressure (i.e. the particle rearrangement stage).

The evidence for a grain boundary transport mechanism, in conjunction with the observed proportionality between $\%\rho_{th}$ and ℓn time with different slopes for different temperatures, suggests that the proposed intermediate stage sintering models are inadequate. In addition, extensive microstructural studies[29] contradict various assumptions of the models[23-26] which lead to the derivation of a semi-logarithmic relationship between $\%\rho_{th}$ and time. These include a failure to observe (1) cubic grain growth kinetics and (2) pore coalescence. These factors will be covered in a later part of this series.

V. Summary and Conclusions

The densification behavior of mullite - containing powders was studied over a range of chemical compositions (Al_2O_3/SiO_2 ratio). Very rapid densification was observed in compositions containing large amounts of liquid phase. This was consistent with an extensive particle rearrangement stage which did not occur in the intermediate group of compositions. A glass phase, however, persisted up to ~74 wt% Al_2O_3 presumably because of

metastable behavior driven by a lowering of high mullite-mullite interfacial energies. A sharp decrease in densification rate was observed upon transition from the mullite solid solution range to the mullite and alumina phase region. This decrease was associated with the elimination of the residual glassy phase.

The time dependence of densification for compositions in the range of 73-75 wt% Al_2O_3 followed a semi-logarithmic relationship between $\%\rho_{th}$ and time. The apparent primary mechanism of densification was grain boundary transport or diffusion whose rate was significantly dependent on the presence or absence of the glassy film. Currently available models for intermediate stage sintering were found to be inadequate for these systems. In general, there is a lack of fundamental understanding regarding the factors which control the time dependence of intermediate stage densification.

ACKNOWLEDGMENT

The support of the Division of Materials Research of the National Science Foundation under Grant No. DMR 79-16891-ZF is gratefully acknowledged. Also thanks are extended to the Materials and Molecular Research Division of the Lawrence Berkeley Laboratory, supported by the Director, Office of Energy Research, Office of Basic Energy Sciences, Materials Science Division of the U.S. Department of Energy under Contract No. DE-AC03-76SF00098.

REFERENCES

1. P. C. Dokko, J. A. Pask, and K. S. Mazdiyasni, "High Temperature Mechanical Properties of Mullite Under Compression," J. Am. Ceram. Soc., 60 [3-4] 150-155 (1977).
2. K. S. Mazdiyasni and L. M. Brown, "Synthesis and Mechanical Properties of Stoichiometric Aluminum Silicate (Mullite)," J. Am. Ceram. Soc., 55 [11] 548-552 (1972).
3. M. D. Sacks, "Correlation of Microstructure of Sintered Mullite Bodies with their Stress-Strain Behavior in Compression Loading at 1200 C," (M. S. Thesis), University of California, Berkeley, LBL-6205 (1977).
4. J. A. Pask et.al., "Structure, Strength, and Corrosion Resistance of Aluminum Silicate Materials," Department of Materials Science and Mineral Engineering, University of California, Berkeley (1977).
5. R. Penty, "Pressure-Sintering Kinetics and Mechanical Properties of High-Purity, Fine-Grained Mullite," (Ph.D. Thesis), Lehigh University (1972).
6. M. D. Sacks, "Sintering Behavior of Mullite-Containing Materials," (Ph.D. Thesis), University of California, Berkeley, LBL-10372 (1979).
7. M. D. Sacks and J. A. Pask, "Sintering of Mullite," in Processing of Crystalline Ceramics (edited by H. Palmour III, R. F. Davis, and T. M. Hare), Plenum Press, New York, pp. 193-203, 1978.
8. W. H. Taylor, "Structure of Sillimanite and Related Minerals," J. Soc. Glass Technol., 16 [62] 111-207 (1932).
9. C. W. Burnham, Year-book Carnegie Inst., 62 158 (1963), 63, 223 (1964).
10. W. Von Lohre and H. Urban, "Contribution to the Morphology of Mullite," Ber. Deut. Keram. Ges., 37 249-251 (1960).

11. I. A. Aksay, "Diffusion and Phase Relationship Studies in the Alumina-Silica System," (Ph.D. Thesis), University of California, Berkeley, LBL-1403 (1973).

12. S. H. Risbud, "Metastability and Crystallization Studies in the Silica-Alumina System," (Ph.D. Thesis), Univeristy of California, Berkeley, LBL-5443 (1976).

13. V. F. Draper, "Mullite Phase Equilibria in System: CaO - Al_2O_3 - SiO_2," (M.S. Thesis), University of California, Berkeley, LBL-5706 (1976).

14. R. L. Coble, "Sintering Crystalline Solids: II," J. Appl. Phys., 32 [5] 793-799 (1961).

15. R. L. Coble and T. K. Gupta, pp. 423-441 in Sintering and Related Phenomena (edited by G. C. Kuczynski, N.A. Hooton, and C. F. Gibbon), Gordon and Breach, Science Publishers, Inc., New York, 1967.

16. T. E. Clare, "Sintering Kinetics of Beryllia," J. Am. Ceram. Soc., 48 [3] 159-165 (1966).

17. R. A. Brown, "Sintering in Very Pure Magnesium Oxide and Magnesium Oxide Containing Vanadium," Bull. Am. Ceram. Soc., 44 [6] 483-487 (1965).

18. C. A. Bruch, "Sintering Kinetics for the Lucalox Alumina Process," General Electric Report No. 61-RL-2778M, (1961).

19. M. J. Bannister, "Interdependence of Pore Removal and Grain Growth During Later Stages of Sintering in Beryllium Oxide," 581-605 in Sintering and Related Phenomena (edited by G. C. Kuczynski, N. A. Hooton, and C. F. Gibbon), Gordon and Breach, Science Publishers, Inc., New York, (1967).

20. B. Wong and J. A. Pask, "Experimental Analysis of Sintering of MgO Compacts," J. Am. Ceram. Soc., 62 [3-4] 141-146 (1979).

21. G. C. Kuczynski, "Statistical Theory of Pore Shrinkage and Grain Growth During Powder Compact Densification," 223-245 in Ceramic Microstructures '76 (edited by R. M. Fulrath and J. A. Pask), Westview Press, Boulder, Colorado, (1977).

22. D. L. Johnson, "A General Model for the Intermediate Stage of Sintering," J. Am. Ceram. Soc., 53 [10] 574-577 (1970).

23. R. L. Coble, "Sintering Crystalline Solids, I. "Intermediate and Final State Diffusion Models," J. App. Phys. 32 [5] 787-792 (1961).

24. J. H. Rosolowski and C. Greskovich, "Theory of the Dependence of Densification on Grain Growth During Intermediate - Stage Sintering," J. Am. Ceram. Soc., 58 [5-6] 177-181 (1975).

25. W. Beere, "The Second Stage Sintering Kinetics of Powder Compacts," Acta. Met. 23 139-145 (1975).

26. B. Wong and J. A. Pask, "Models for Kinetics of Solid State Sintering," J. Am. Ceram. Soc., 62 [3-4] 138-141 (1979).

27. T. Ikegami et.al., "A Model of Densification with Simultaneous Grain Growth," J. Appl. Phys., 49 7 (1978).

28. W. D. Kingery, "Densification During Sintering in the Presence of a Liquid Phase. I. Theory," J. Appl. Phys. 30 [3] 301-306 (1959).

29. M. D. Sacks and J. A. Pask, to be published.

30. I. A. Aksay and J. A. Pask, "Stable and Metastable Equilibria in the System SiO_2 - Al_2O_3," J. Am. Ceram. Soc., 58 [11-12] 507-512 (1975).

Table 1. Characteristics of A-14/SiO_2 Calcined and Ground Powders

Composition	Surface Area (m^2/g)	X-ray Diffraction (phases present)
60IP	1.9	Mullite
73IP	1.8	Mullite
73PP	2.1	Mullite (major)
		α - Al_2O_3 (trace)*
75PP	1.7	Mullite (major)
		α - Al_2O_3 (minor)

*Contamination during grinding.

Table 2. Compressive Strength at Elevated Temperatures of Several Compositions

Composition	Ultimate Engineering Stress (MN/m^2)	% Theoretical Density	Mean Grain Size (μm)
71.8IP*	630	95	4.5
73IP*	755	95	4.5
74IP*	815	93	7
75IP*	620	83	4
71.8IP†	250	95	4.5
74IP†	610	93	7

*Test temperature - 1200 C, †test temperature - 1400°C.

FIGURE CAPTIONS

Fig. 1. Equilibrium SiO_2 - Al_2O_3 phase diagram according to Aksay and Pask.[30]

Fig. 2. Plots of percent of theoretical density versus overall chemical composition (wt% Al_2O_3) for samples sintered at 1700°C for 1, 4, and 12 hrs.

Fig. 3. Two phase (mullite and aluminum silicate glass) microstructures for overall 60 and 65 wt% Al_2O_3 compositions formed during sintering.

Fig. 4. Percent of theoretical density vs. time plots at 1660°C for 60IP, 73IP, 73PP, and 75IP.

Fig. 5. Percent of theoretical density vs. ℓn time plots (1540°C - 1730°C) for 73IP.

Fig. 6. Percent of theoretical density vs. ℓn time plots (1540°C - 1730°C) for 73PP.

Fig. 7. Percent of theoretical density vs. ℓn time plots (1540°C - 1730°C) for 75IP.

Fig. 8. Plot of open porosity (%) vs. total porosity (%) for 73IP samples sintered at 1540°C - 1730°C.

Fig. 9. Microstructures of "IP" compositions ranging from 71.8 to 75 wt% Al_2O_3 which were sintered at 1700°C for 12 hrs.

Fig. 10. Transmission electron micrographs of 73IP microstructure indicating the presence of small amounts of glass phase. (Taken by W. Kriven in this laboratory.)

Fig. 11. Microstructure for 73IP sample sintered for 1 hr at 1580°C which shows an Al_2O_3 particle (hexagonal shaped grain in the center) that was detected by EDAX.

Fig. 12. A: Microstructure of 71.8IP, sintered at 1700°C for 8 hrs, showing small glassy areas (circled) and occasional larger regions (center).

B: Microstructure of 75 wt% Al_2O_3 sample, sintered at 1700°C for 8 hrs in which glass phase is not detected.

Fig. 13. Microstructure of 71.8IP sintered for 100 hrs at 1700°C showing the coalescense of glass phase into large "pockets," after a light HF solution etch.

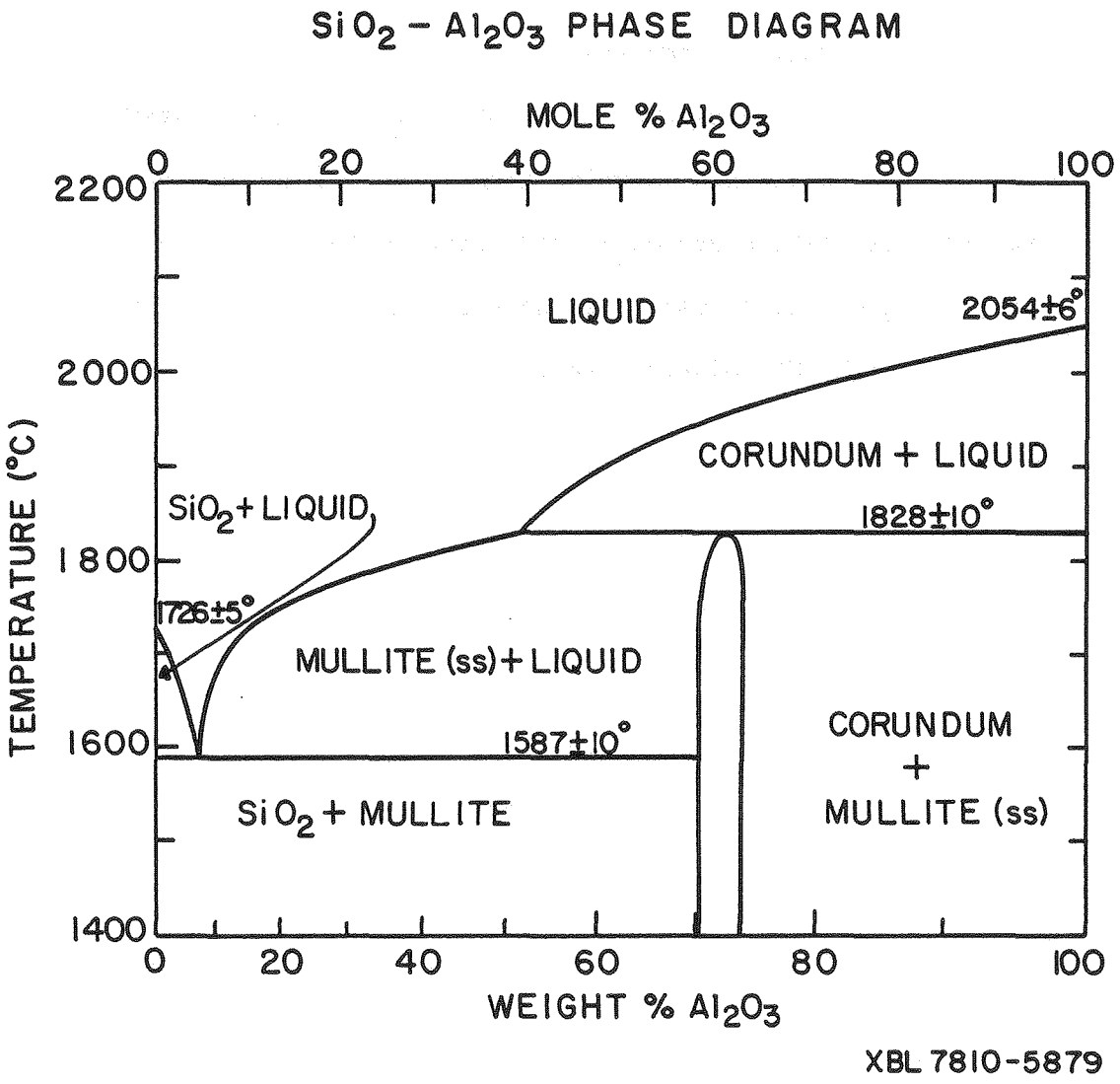
SiO2 – Al2O3 PHASE DIAGRAM
MOLE % Al2O3
0
20
40
60
80
100
2200
2000
1800
1600
1400
TEMPERATURE (°C)
LIQUID
2054±6°
CORUNDUM + LIQUID
SiO2 + LIQUID
1828±10°
1726±5°
MULLITE (ss) + LIQUID
1587±10°
CORUNDUM
+
MULLITE (ss)
SiO2 + MULLITE
WEIGHT % Al2O3
XBL 7810-5879

Fig. 1

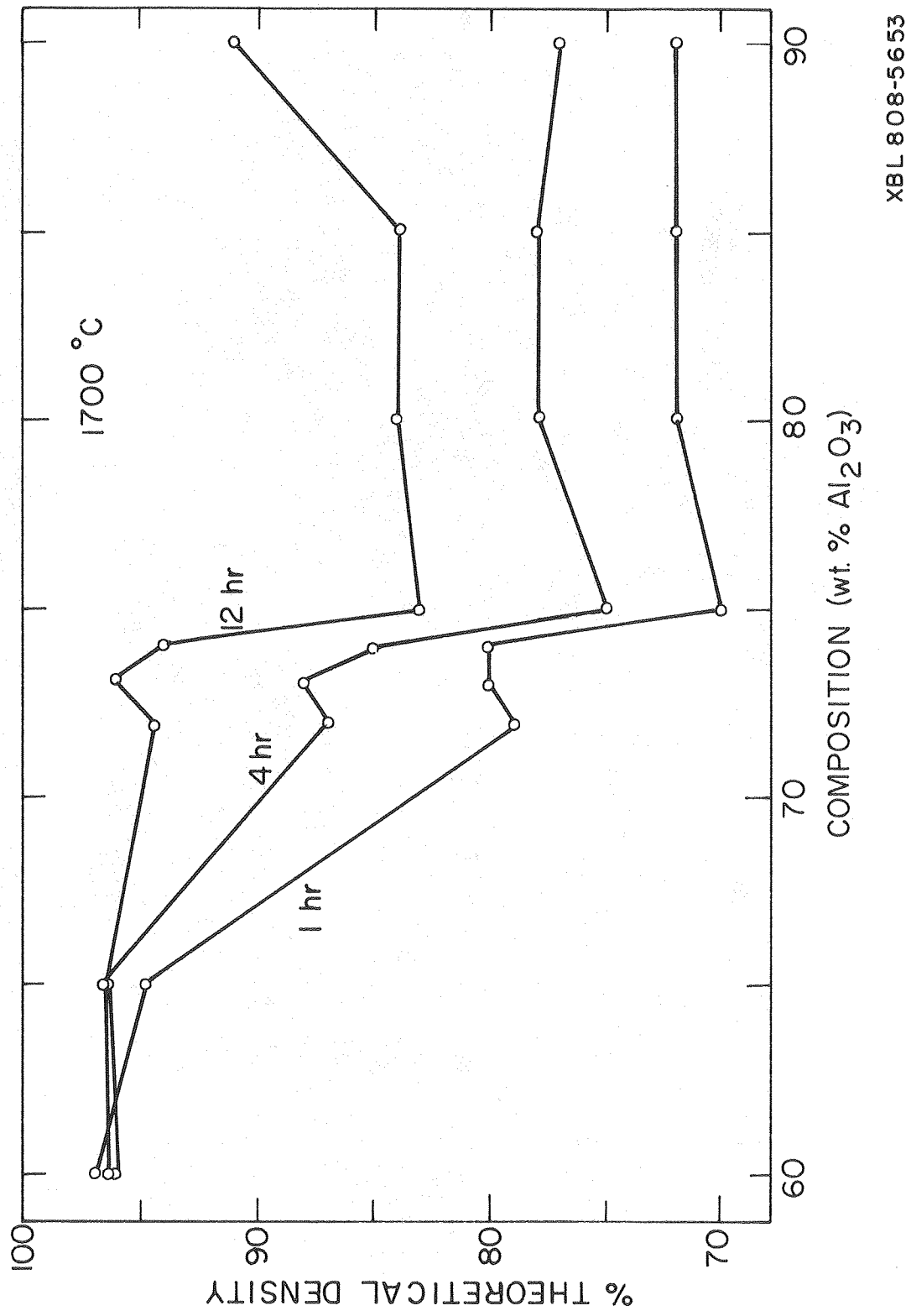
% THEORETICAL DENSITY
100
90
80
70
60
90
80
70
COMPOSITION (wt. % Al_2O_3)
1700 °C
12 hr
4 hr
1 hr
XBL 808-5653

Fig. 2

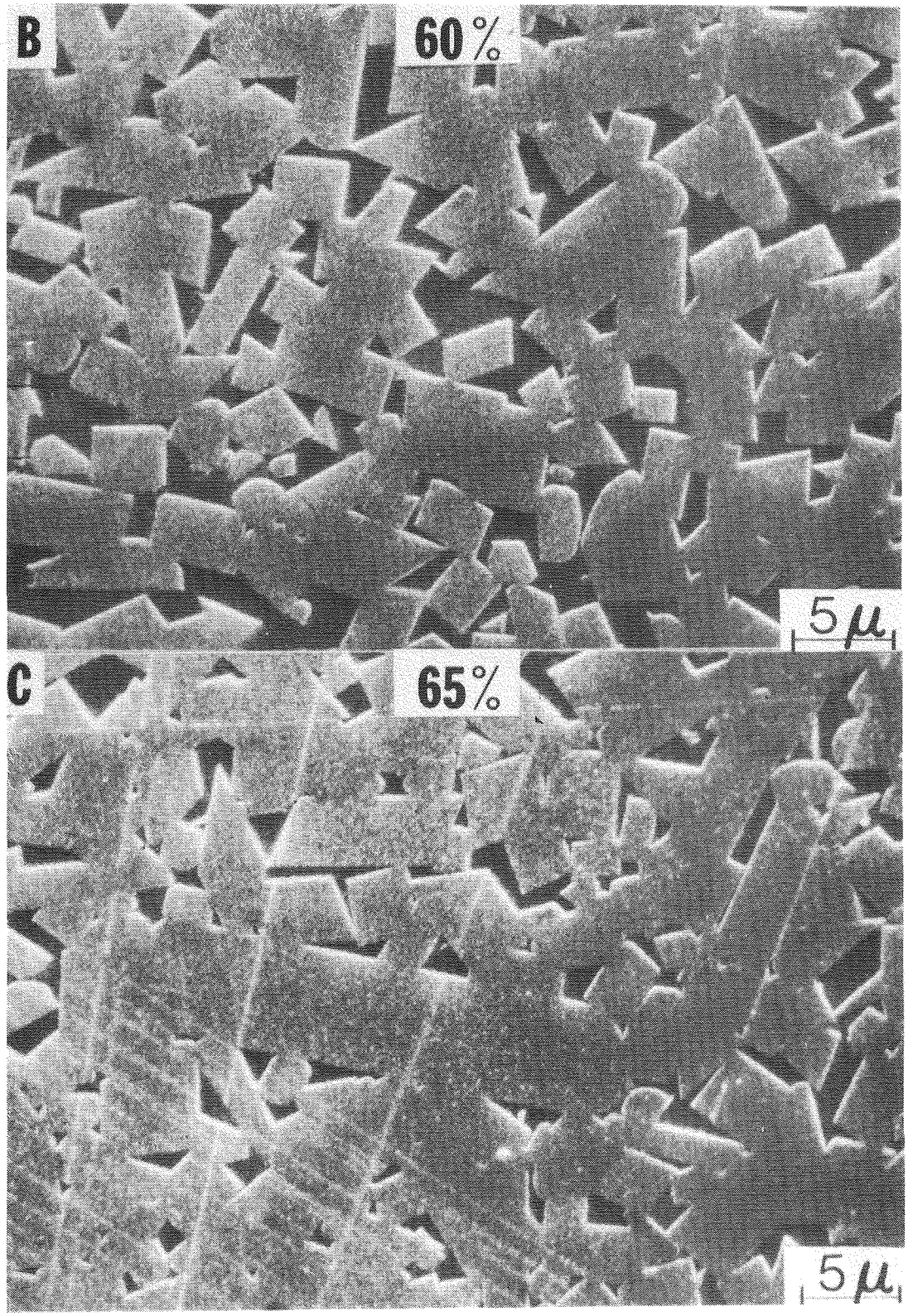

Fig. 3

XBB 790-16635

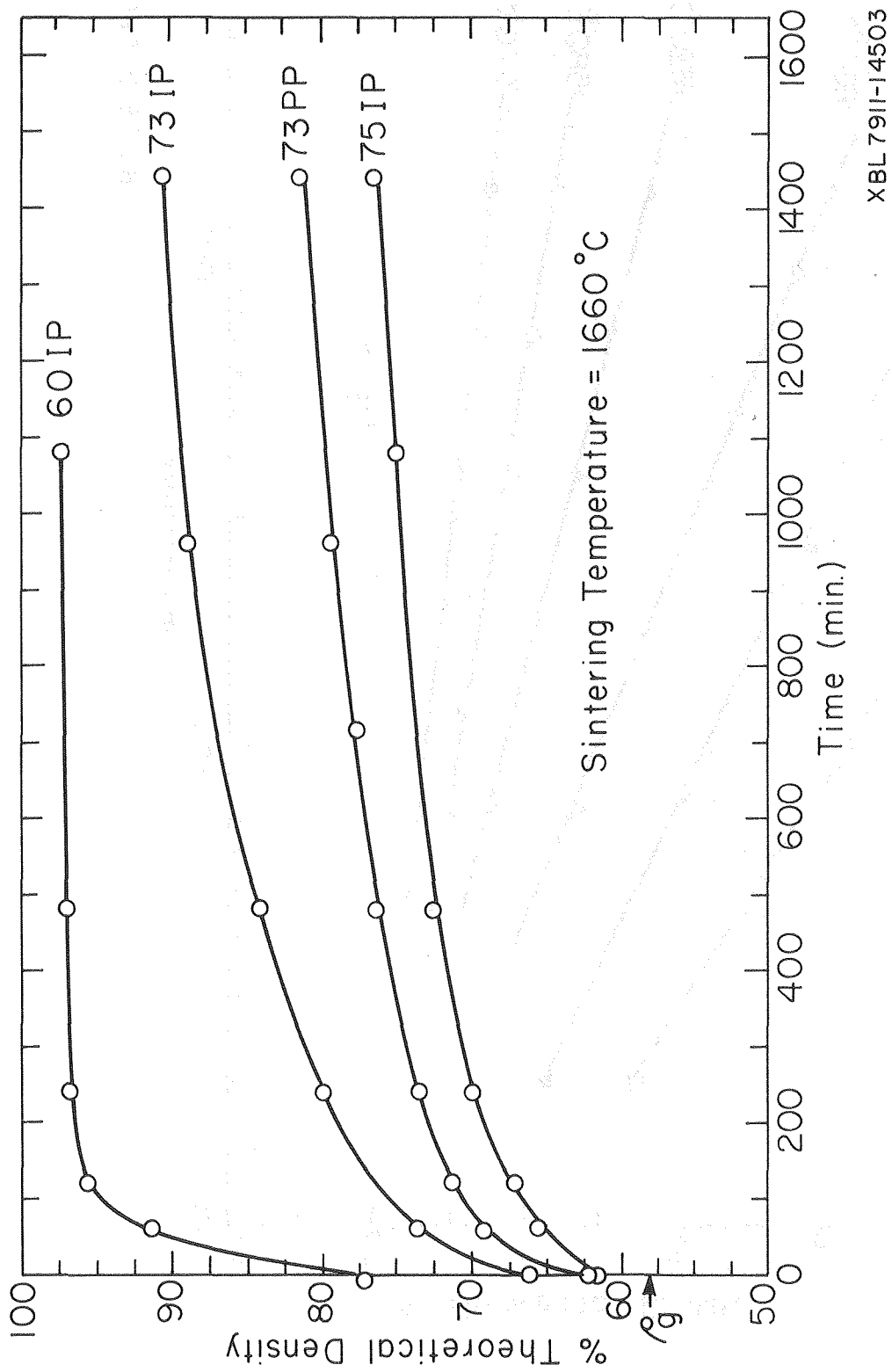

XBL 7911-14503

Fig. 4

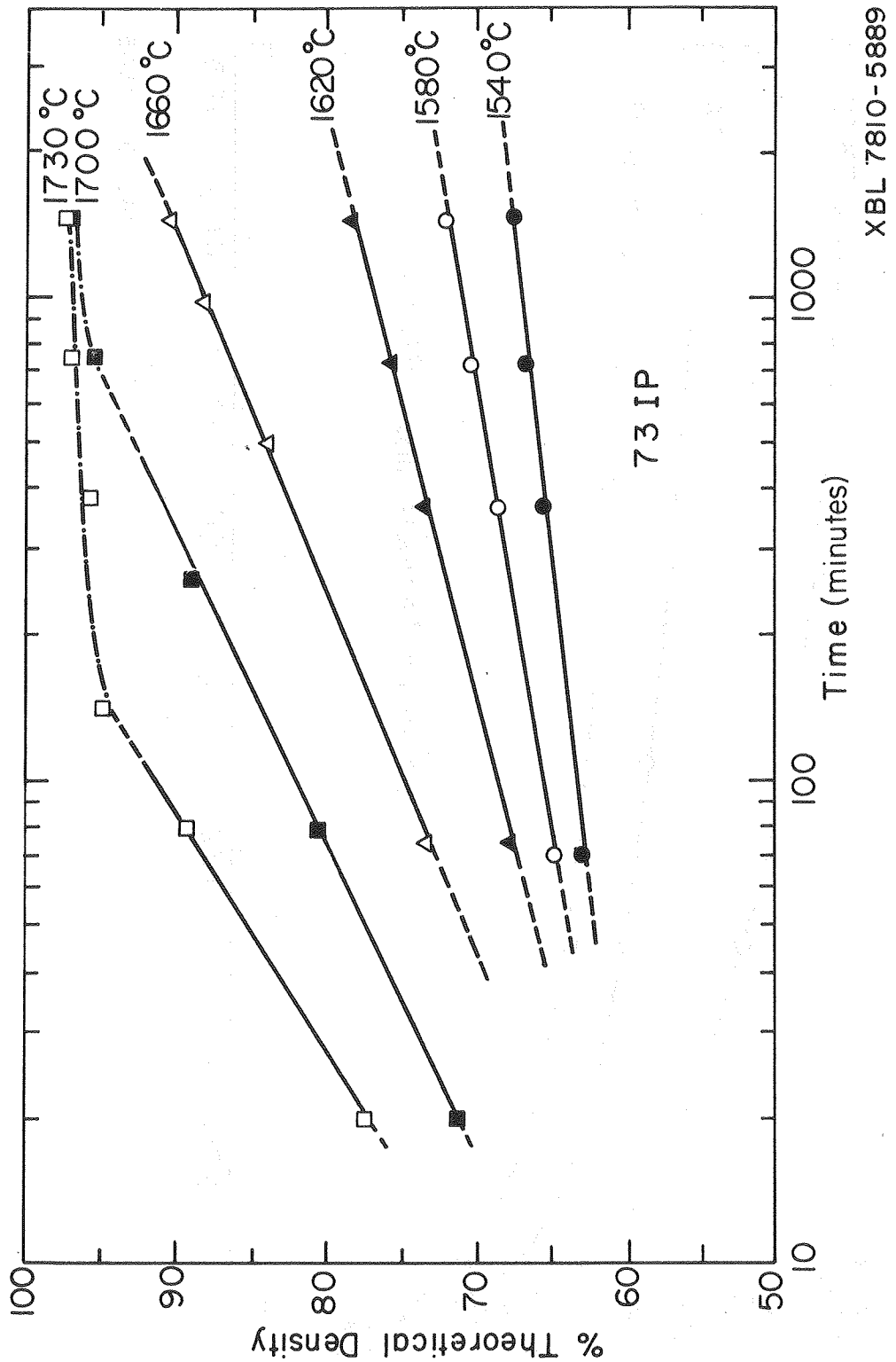
% Theoretical Density
100
90
80
70
60
50
10
100
1000
Time (minutes)
1730 °C
1700 °C
1660 °C
1620 °C
1580 °C
1540 °C
73 IP
XBL 7810-5889

Fig. 5

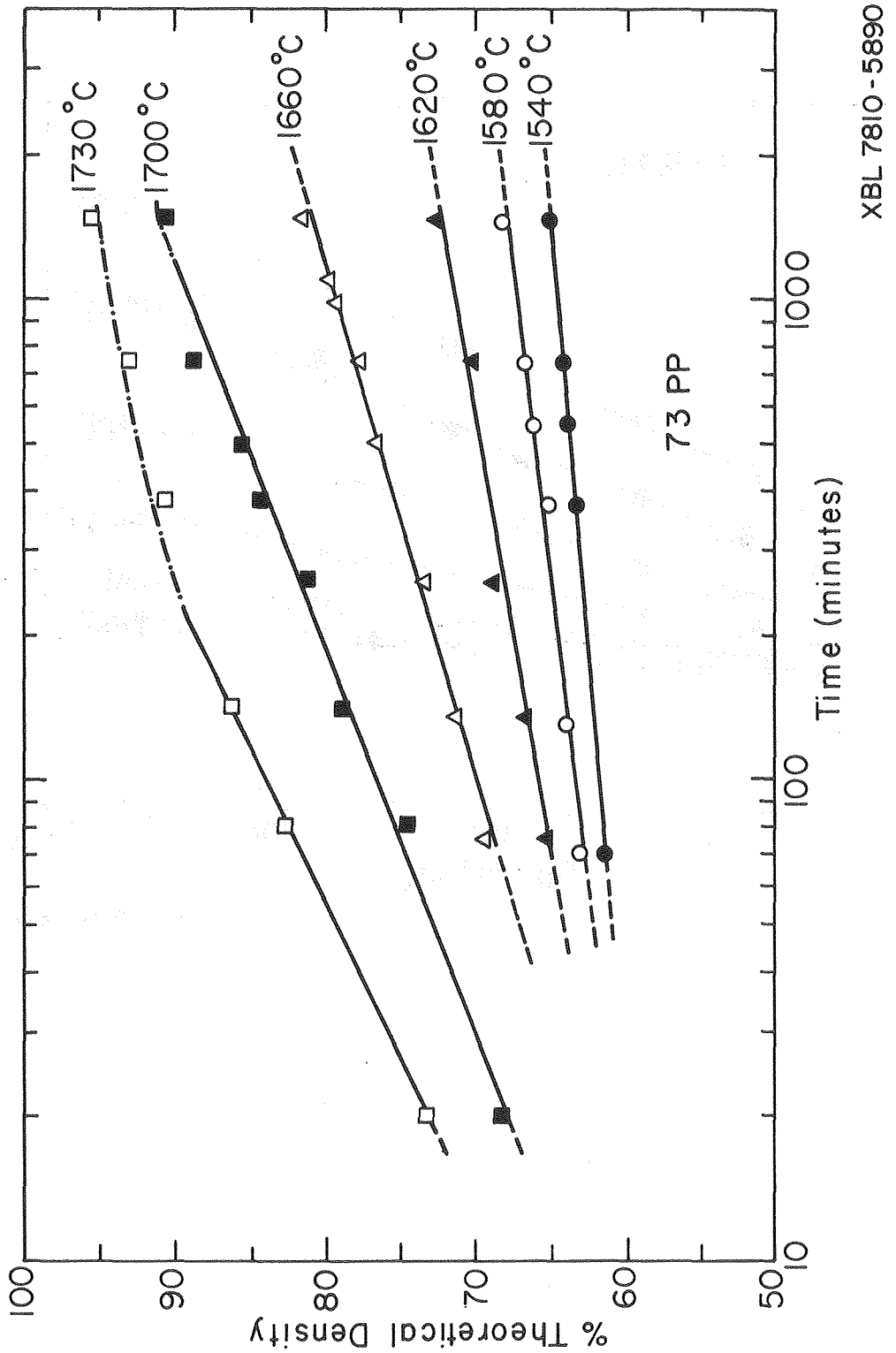
% Theoretical Density
100
90
80
70
60
50
10
100
1000
Time (minutes)
73 PP
1730°C
1700°C
1660°C
1620°C
1580°C
1540°C
XBL 7810-5890

Fig. 6

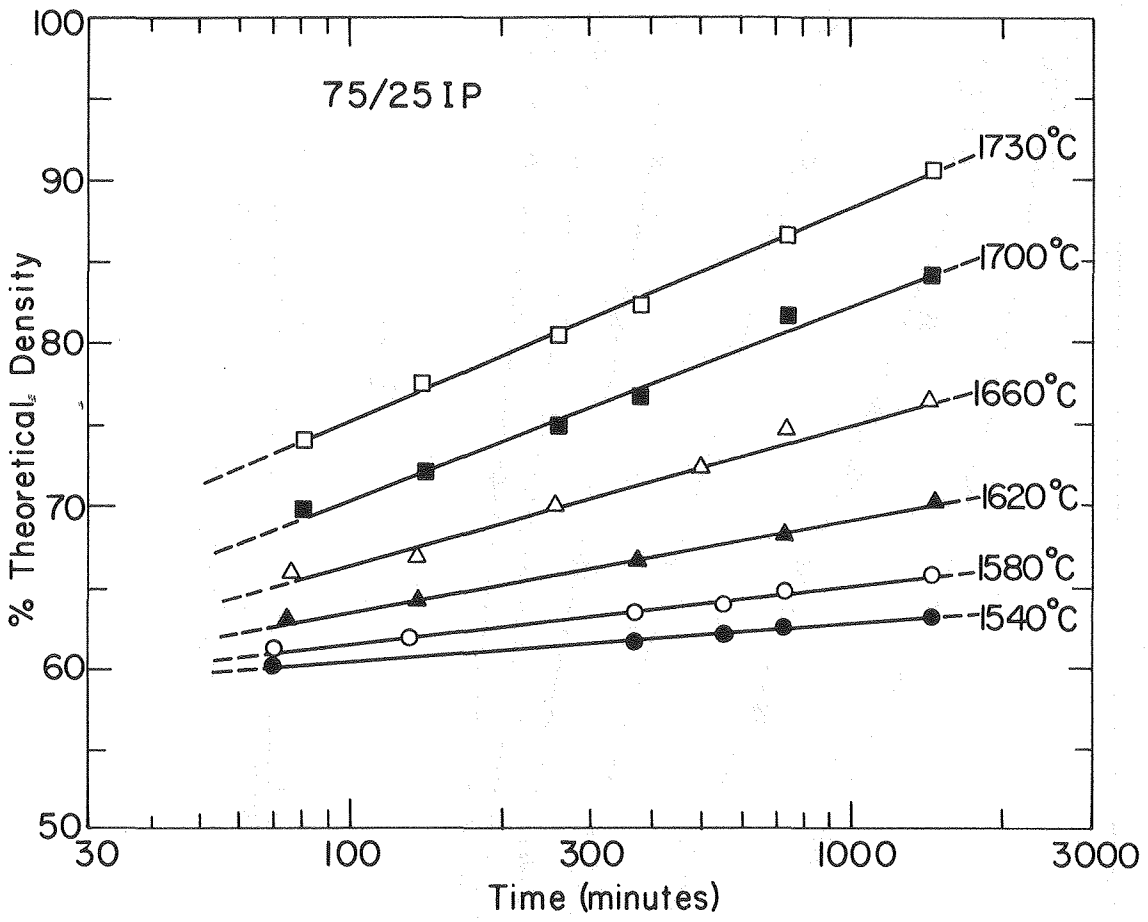
75/25 IP
1730°C
1700°C
1660°C
1620°C
1580°C
1540°C
% Theoretical Density
Time (minutes)
100
90
80
70
60
50
30
100
300
1000
3000
XBL 7810-5894

Fig. 7

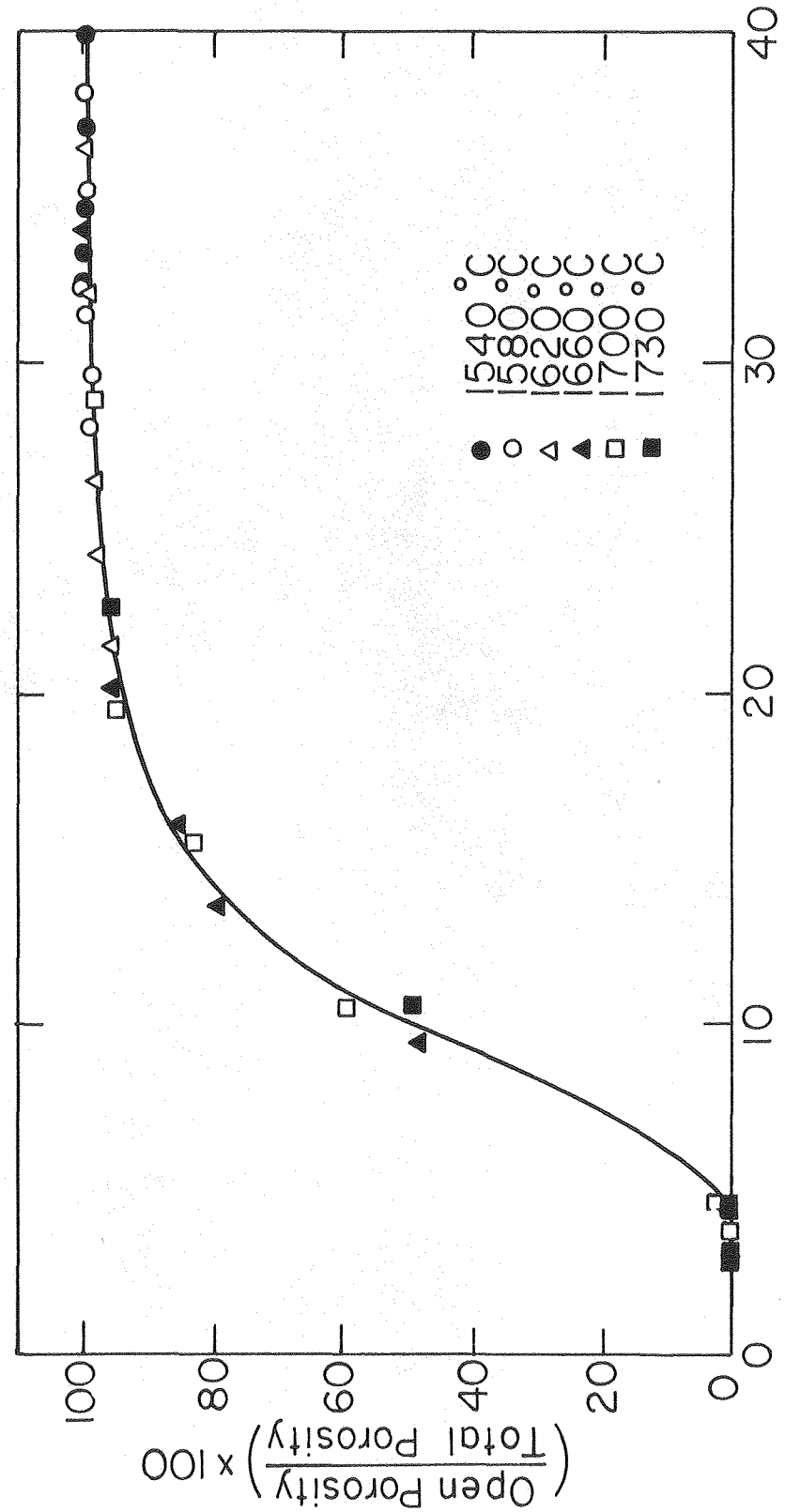

XBL 7911-14518

Fig. 8

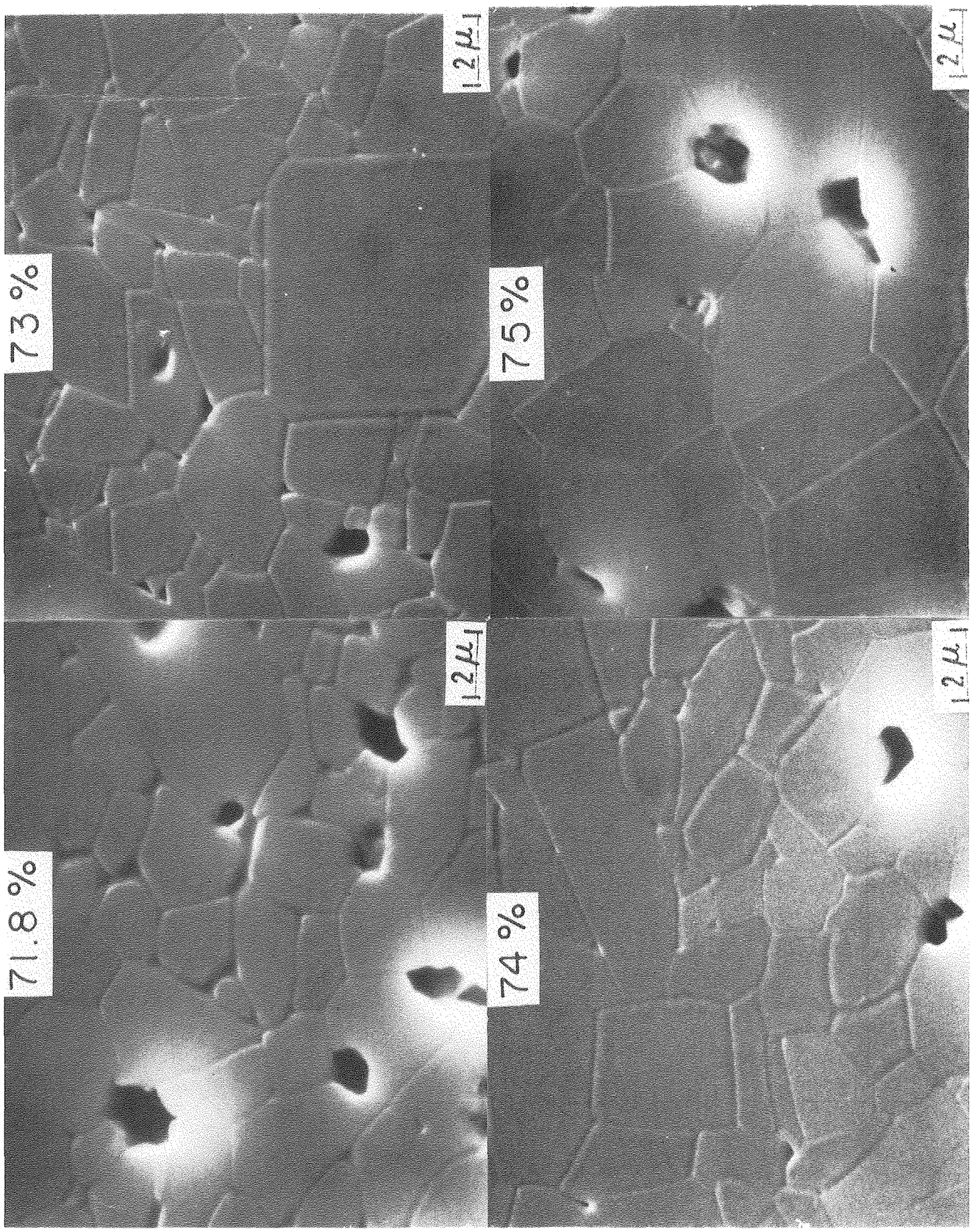

XBB770-10662

Fig. 9

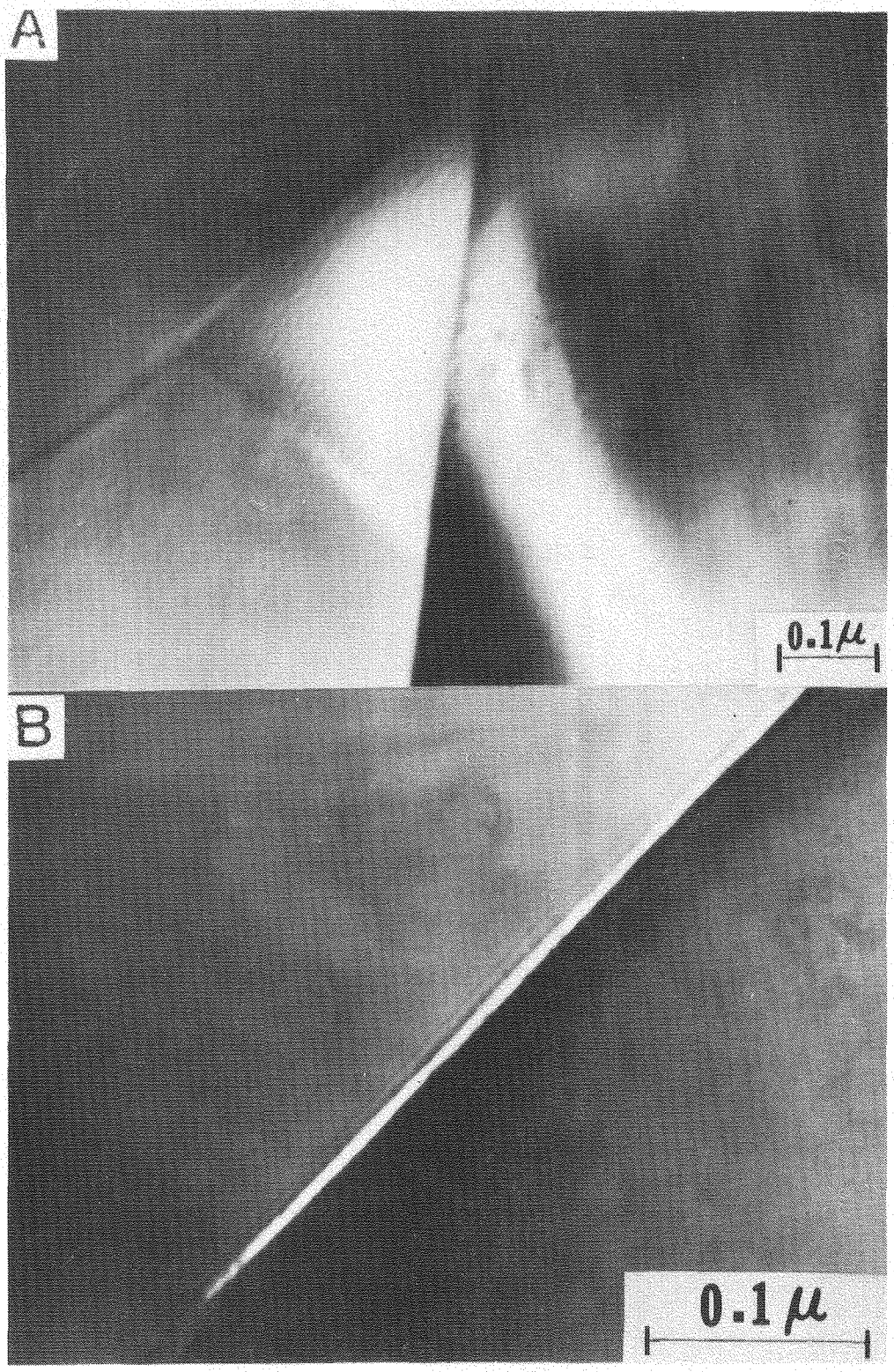

Fig. 10

XBB 760-10655

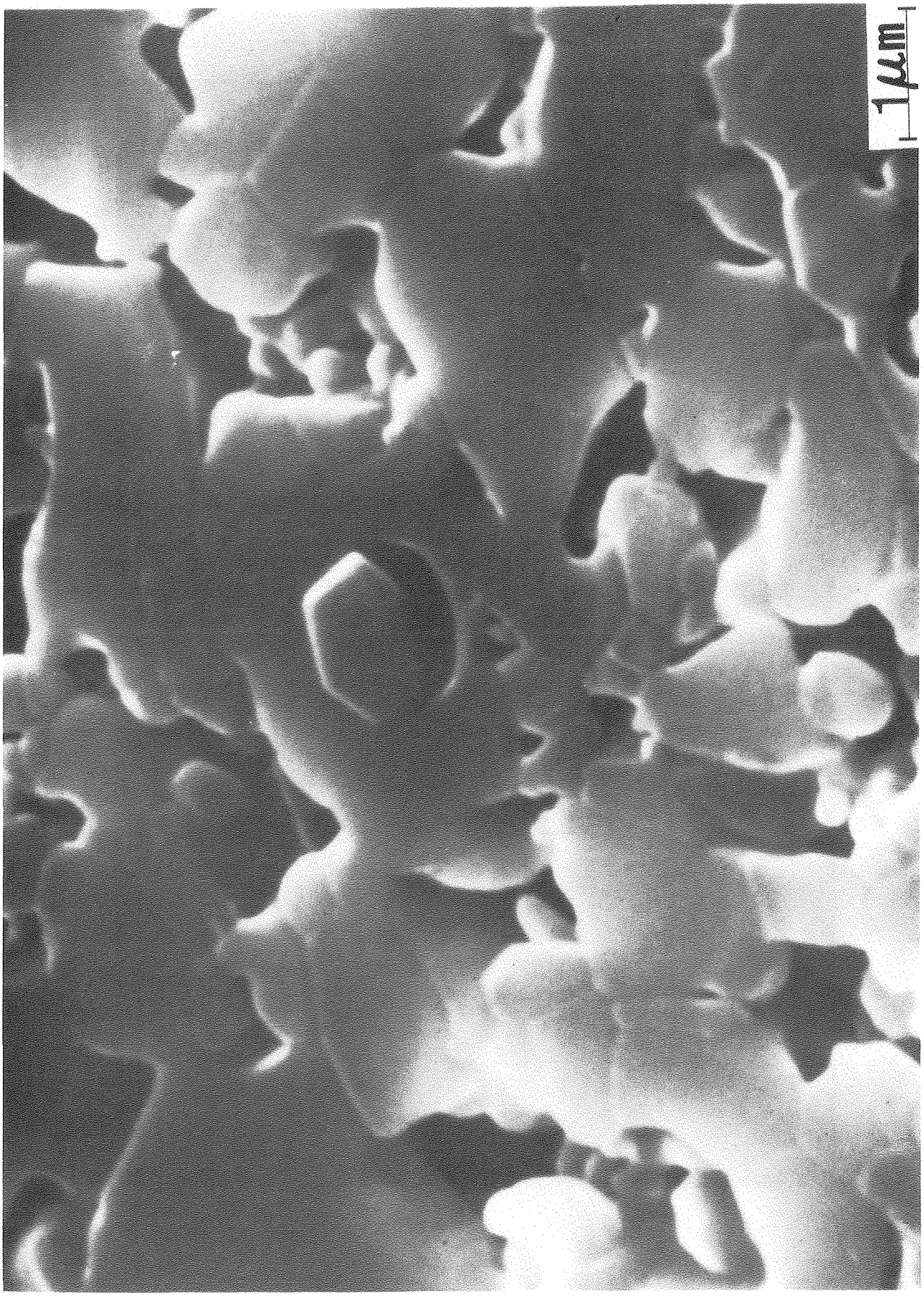

XBB790- 15979

Fig. 11

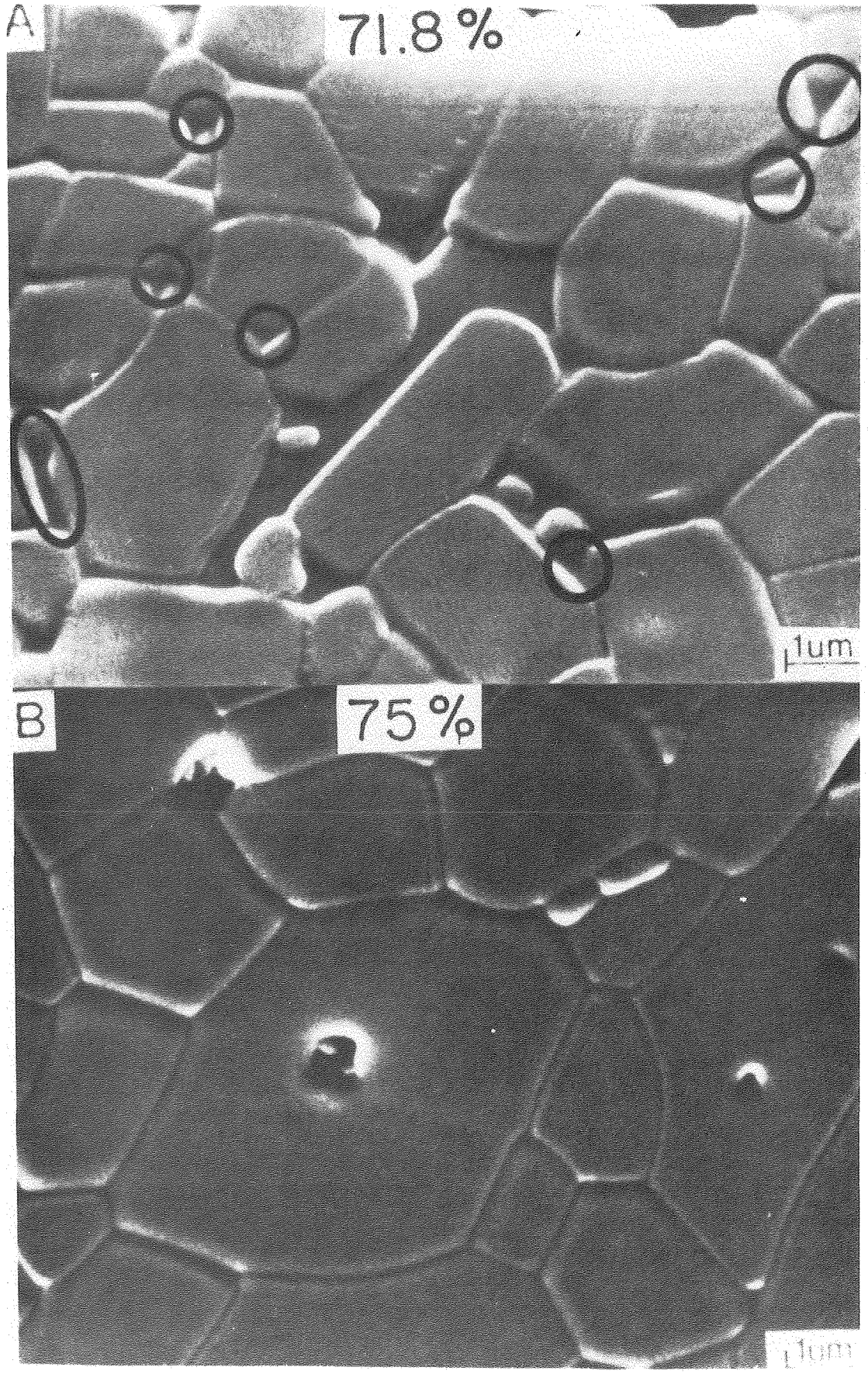

Fig. 12

XBB 770-11029A

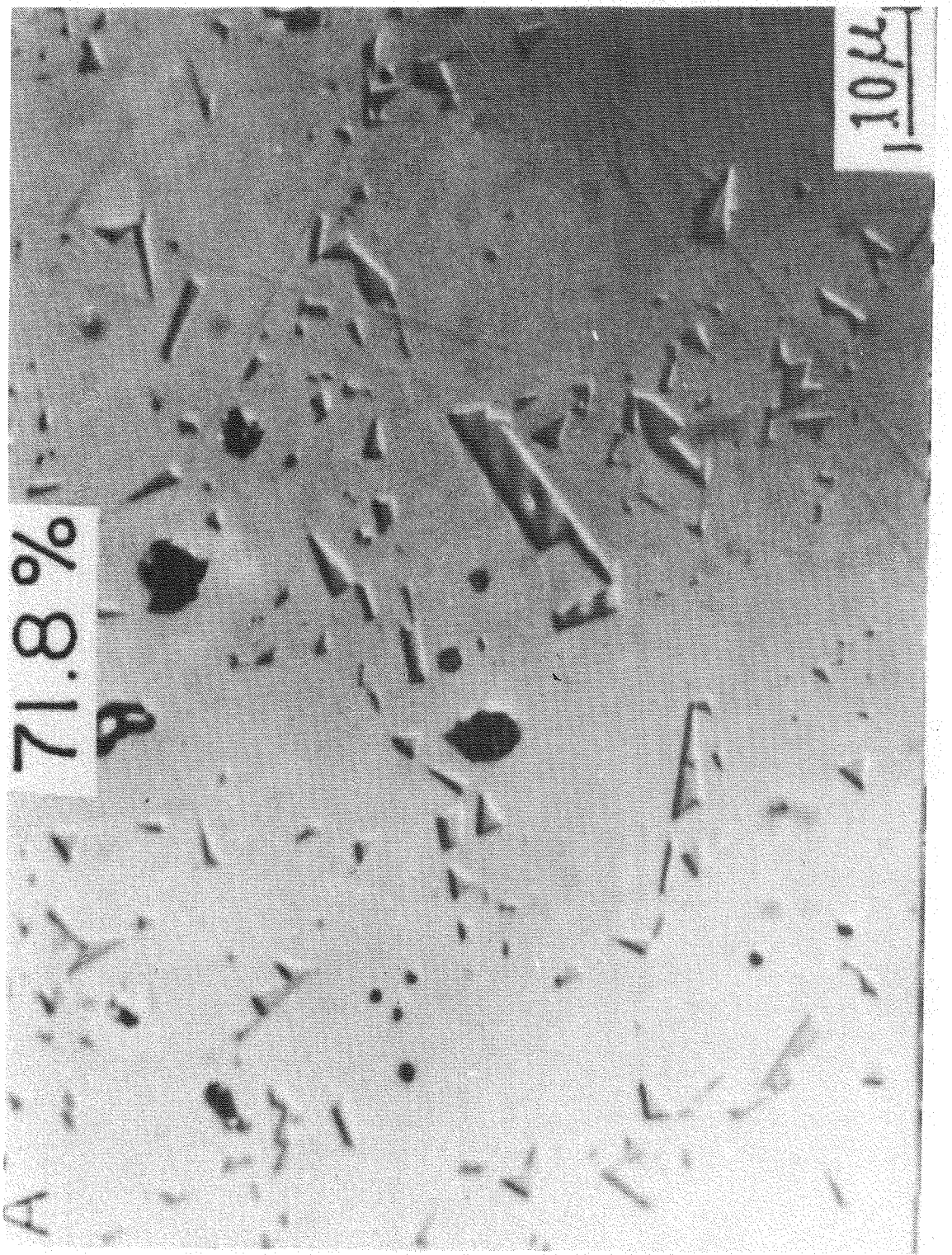

XBB 770-11029B

Fig. 13